

# The posterior cruciate ligament: a study on its bony and soft tissue anatomy using novel 3D CT technology

Tom Van Hoof · Michiel Cromheecke ·  
Thomas Tampere · Katharina D'herde ·  
Jan Victor · Peter C. M. Verdonk

Received: 15 January 2012 / Accepted: 27 November 2012 / Published online: 27 December 2012  
© Springer-Verlag Berlin Heidelberg 2012

## Abstract

**Purpose** The bony insertion sites of the PCL have been studied and described extensively using 2D technology such as macroscopic images, plain radiograph, computerized tomography (CT) and MRI. The purpose of this study is to visualize both the tibial and the femoral bony insertion sites but also the soft tissue anatomy of the native PCL using novel 3D CT imaging. In addition, new concepts of best-fit cylinder and central axis are introduced and evaluated.

**Methods** Nine unpaired knees of embalmed cadavers were used in this study. Following the dissection process, the PCL was injected with a contrast medium for computed tomography (CT) imaging. The obtained CT images were segmented and rendered in 3D allowing morphological and morphometric analysis of PCL. Femoral and tibial footprint surface area, best-fit PCL-cylinder intersection area, best-fit PCL-cylinder/footprint coverage ratio, best-fit PCL-cylinder central axis projections at the tibial and femoral footprint were used to describe the anatomy of the PCL.

**Results** Mean footprint surface area of the tibial and femoral footprint were 189.1 and 293.3 mm<sup>2</sup>, respectively. The mean diameter of the best-fit cylinder was 10.5 mm. The mean coverage of the best-fit cylinder on the tibial and femoral footprint was 76.5 and 46.5, respectively. The best-fit cylinder central axis was located in the anterolateral AL bundle footprint on the femur and more centrally in the PCL footprint on the tibia.

**Conclusion** This study is the first to describe the detailed anatomy of the human PCL with respect to its course and footprints using a 3D approach. It confirms the large difference between the tibial and the femoral footprint area with the former being significantly smaller. In addition, a large inter-patient variability is observed. The best-fit cylinder and central axis concept offer additional insights into the optimal tunnel placement at the tibia and femoral footprint in order to cover the largest portion of the native PCL soft tissue.

**Keywords** Posterior cruciate ligament · 3D-computerized tomography · Anatomy

T. Van Hoof · K. D'herde  
Department of Anatomy,  
Ghent University, Ghent, Belgium

M. Cromheecke · T. Tampere · J. Victor  
Department of Orthopaedic Surgery and Traumatology,  
Ghent University, Ghent, Belgium

P. C. M. Verdonk  
Department of Physiotherapy and Orthopaedic Surgery,  
Faculty of Medicine, Ghent University, Ghent, Belgium

P. C. M. Verdonk (✉)  
Department of Orthopaedic Surgery, Monica Hospitals,  
Harmoniestraat 68, 2018 Antwerpen, Belgium  
e-mail: pverdonk@yahoo.com

## Introduction

The strongest ligament in the knee, the posterior cruciate ligament (PCL), arises from the medial aspect of the medial femoral condyle and inserts posterior to the intercondylar eminence of the tibia.

The insertion sites of the PCL have been studied and described extensively using 2D technology such as macroscopic images, plain radiograph, computerized tomography (CT) and MRI [1, 3, 5, 7, 9, 15, 19–21].

Recently, 3D imaging and segmentation technology has been introduced into the orthopaedic field to improve the

comprehension of the complex *osseous* anatomy of the human knee. Such information has led to the better understanding of the bony insertion sites of the native cruciate ligament and has been translated recently into the clinical practice as the anatomical ligament reconstruction concept. The definition of anatomical ligament reconstruction only includes bony references such as the following: a centre-tibial footprint to centre-femoral footprint tunnel position and at least 80 % footprint coverage. This concept, however, does not take into account soft tissue references such as the course and volume of the native ligament, as 3D visualization of *soft tissue* anatomical structures such as the PCL has not yet been performed using CT images [2, 14].

The purpose of this study is to visualize both the tibial and femoral bony insertion sites but also the soft tissue anatomy of the native PCL using novel 3D CT imaging. In addition, new concepts of best-fit cylinder and central axis are introduced and evaluated. The central axis represents the best-fit cylinder around the native PCL fibres as determined by an automated computerized process. The central axis bony insertion therefore depicts the ideal tunnel position to enclose the bulk of the PCL fibres. This information can be useful for ligament reconstructive purposes [2, 8, 11, 12, 16, 18, 23, 24].

## Materials and methods

Nine unpaired knees of embalmed cadavers (four from male cadavers and five from female cadavers) with no macroscopic degenerative or traumatic changes were used in this study. The mean age of the cadavers, at the time of death, was 79.4 years (range, 66–97 years).

### Procedure

The knees were carefully dissected through anterior and posterior approach. For anterior approach, the knee was positioned in 90° of flexion and the patellar ligament was sectioned transversely at the level of the joint space. The infrapatellar fat tissue and the synovial sleeve embedding the PCL were carefully removed.

For the posterior approach, the knee was fully extended. In the popliteal fossa, the heads of the gastrocnemius muscles, the tendon of the semimembranosus muscle and deep popliteal neurovascular bundle were excised to the level of the oblique and the arcuate popliteal ligament and the popliteus muscle. The popliteal tendon was transected at its most lateral visible part where it disappears under the edge of the capsule. From this transection point, the posterior capsule was transversely opened until the tibial and femoral insertion sites of the PCL were clearly visible and

accessible. The synovial sleeve was removed, and the posterior meniscomfemoral ligament was kept intact. The anterior approach, craniomedially to the ACL, was integrated in the anatomical procedure for optimal accessibility of the femoral insertion site of the PCL. The dissection procedure (anterior and posterior approach) was performed with the preservation of the lateral and medial parts of the capsule in the manner that rotational stability was maintained in positioning the knee during CT scanning.

Following the dissection process, the PCL was injected with a contrast medium for computed tomography (CT) imaging, consisting of 80 % Barium sulphate, 10 % glycerine, 10 % water. Toluidine blue powder (0.1 g) was added to stain the solution which allows a visual control over dispersion and possible leakage of the mixture [6, 17, 22]. A needle (Terumo® needle 0.45 × 23 mm) was inserted between the collagen fibres of the PCL, and the solution was injected with mild pressure until leakage occurred at the injection site or at spots further away along the ligament. Pieces of gauze swabs were wrapped around neighbouring structures and surfaces in order to prevent contamination of possible leaking contrast solution [4].

The injection needle subsequently was directed towards the femoral and tibial insertion site of the PCL as far as the contact point with the bony surface [7, 19]. On this spot, a small bolus of contrast was injected and this was repeated covering the complete insertion area. Then, a solid dissection needle—with identical diameter as the injection needle—was used for repeated pricking in this area to obtain maximal absorption of contrast solution in the bony PCL insertion area (footprint).

Additionally, the accessible exterior parts of the PCL were covered with an ethyl-acetate based solution containing lead dioxide to enhance surface contrast [7, 10, 22].

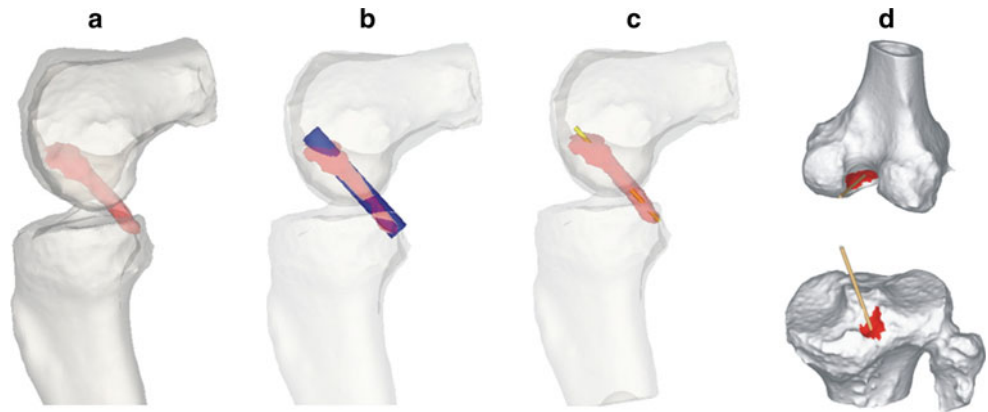
### CT scanning

After anatomical preparation, the specimens were studied by a helical CT scan (Siemens/volume zoom). The obtained CT images were then imported into a software package that is able to process any 2D stack of images (e.g., CT and MRI) and allows 3D reconstruction. In the present study, Mimics 14.11® (Materialise N.V., Heverlee, Belgium) was used for visualization and segmentation of CT images and 3D rendering of the knee joint with and PCL with a direct link to morphological and morphometric analysis of PCL and PCL reconstruction procedures [22].

### Measurements

After the segmentation process, 3D reconstructions were calculated from the selected masks of the native PCL (Fig. 1), the distal part of the femoral shaft with the

**Fig. 1** Three-dimensional representation of PCL, best-fit PCL-cylinder and central axis. **a** 3D reconstruction of PCL (red) in semi-transparent knee; **b** PCL (red) with best-fit PCL-cylinder (blue); **c** PCL (red) with central axis (yellow); **d** tibial (below) and femoral (above) footprints of PCL (red) with intersecting central axis



condyles and the tibial plateau to a few centimetres distal from the tibial tuberosity.

Femoral and tibial footprint surface area, best-fit PCL-cylinder intersection area, best-fit PCL-cylinder/footprint coverage ratio (Table 1) and best-fit PCL-cylinder central axis projections at the tibial (Fig. 2) and femoral (Fig. 3) footprint were used to describe the anatomy of the PCL.

#### Data analysis

Mean (SD) surface areas ( $\text{mm}^2 \pm 1 \text{ SD}$ ) were calculated for the tibial and femoral native PCL insertion site. Then, the mean intersection areas ( $\text{mm}^2 \pm 1 \text{ SD}$ ) of the best-fitted PCL-cylinder with the tibial and femoral footprint surfaces were calculated and expressed as a mean coverage ( $\% \pm 1 \text{ SD}$ ) in relation to the complete footprint areas.

**Table 1** Overview of the individual tibial and femoral footprint surface areas, the individual coverage of the best-fit cylinder on the tibial and femoral footprints in terms of percentage, the diameter of the best-fit cylinder and the femoral epicondylar width for each of the nine knees used

	Tib sfc ( $\text{mm}^2$ )	Fem sfc ( $\text{mm}^2$ )	Tib cov (%)	Fem cov (%)	Diameter (mm)	Fem epw (mm)
Knee 1	263.4	302.1	84.5	38.5	10.8	86.9
Knee 2	190.6	270.7	66.0	54.0	9.7	89.1
Knee 3	257.6	400.5	59.6	47.2	11.9	87.0
Knee 4	68.7	193.7	91.4	37.1	7.5	76.6
Knee 5	186.6	216.2	74.4	48.5	11.0	79.3
Knee 6	115.2	259.6	91.4	50.2	10.1	85.2
Knee 7	191.0	326.6	67.2	48.0	10.6	81.7
Knee 8	202.2	348.4	84.1	54.0	11.6	85.0
Knee 9	226.2	321.7	69.9	40.7	11.1	86.0
Mean	189.1	293.3	76.5	46.5	10.5	84.1

*Tib Sfc* tibial footprint surface area, *Fem Sfc* femoral footprint surface area, *Tib Cov* tibial coverage, *Fem Cov* femoral coverage, *Diameter* diameter of the best-fit cylinder, *Fem Epw* femoral epicondylar width. The data has a normal distribution; Shapiro–Wilk ( $p$  value n.s.)

The areas of the femoral and tibial footprints and native PCL diameter were compared to the femoral epicondylar mediolateral width, using a Spearman's rank correlation coefficient. The level of significance was set at  $p < 0.05$ .

#### Results

Based on anatomical dissection, interpretation of specific collagen tissue contrasted CT, 3D reconstructions of the native PCL, tibial plateau and intersection area, we found that the posterior cruciate ligament was attached to the posterior intercondylar area between the tibial plateaus and posteriorly of the intercondylar eminences.

In line with the topographical studies of Forsythe et al. [7] and Tajima et al. [19], we also found the PCL consisting of two bundles inserting in different planes on the posterior intercondylar area. In almost every 3D native PCL, the anterolateral (AL) and posteromedial (PM) bundle is clearly detectable. Two slopes can be identified on tibial insertion area of the PCL: (1) an anterolateral slope, located at the superolateral aspect of the posterior intercondylar area, to which the AL bundle is attached; (2) a posteromedial slope in the inferomedial aspect of the fossa, which is the insertion area for the PM bundle [1, 5, 11, 13, 19].

In cranial direction, the PCL inserts on the lateral surface of the medial femoral condyle in the intercondylar fossa. This insertion area is bounded caudally by the rim of the articular surface of the medial condyle and cranially by the medial intercondylar ridge depicted in most knee samples. The medial bifurcate ridge, described in Forsythe et al. [7] as a small osseous prominence between the anterolateral and posteromedial bundles of the PCL, was not visible on the bony surfaces of the CT datasets and 3D reconstructions in the current study. On the other hand, it was possible to distinguish the anterolateral and posteromedial bundles in the 3D native PCL at the femoral insertion site [1–3, 5, 11, 13, 15, 19, 20].

**Fig. 2** Three-dimensional representation of the tibial footprint of the native PCL (*red*) for the nine knees used (**a–i**). In *blue* colour, the intersection area of the best-fit PCL-cylinder superimposed on the tibial footprint (*red*), and in *yellow* colour, the osseous intersection of the central axis superimposed on preceding footprint and intersection area (*red* and *blue*)

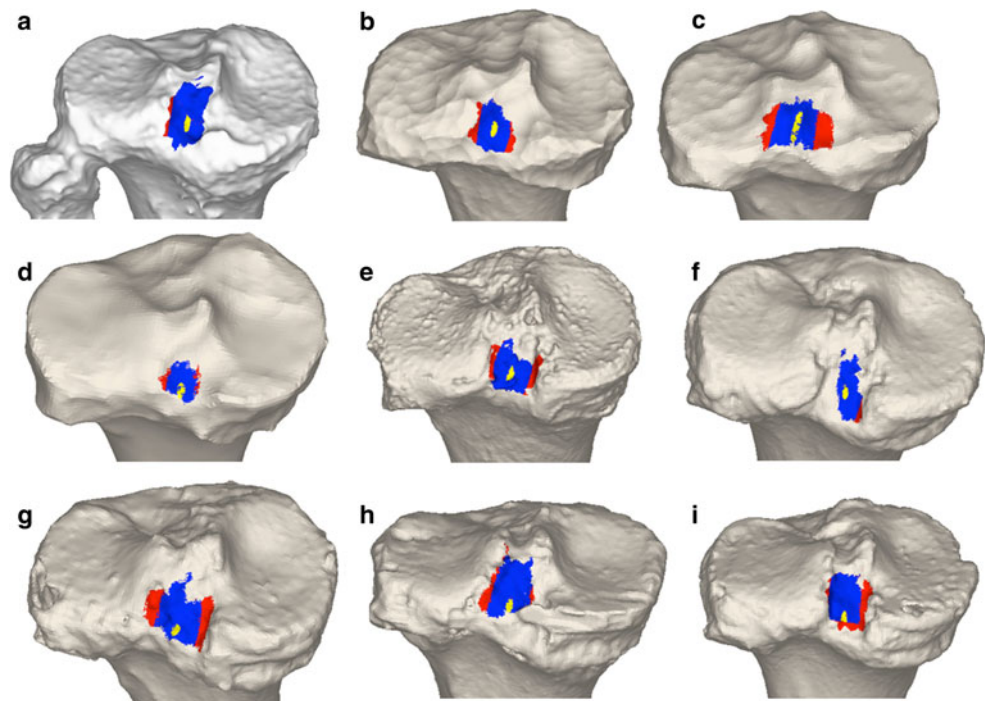
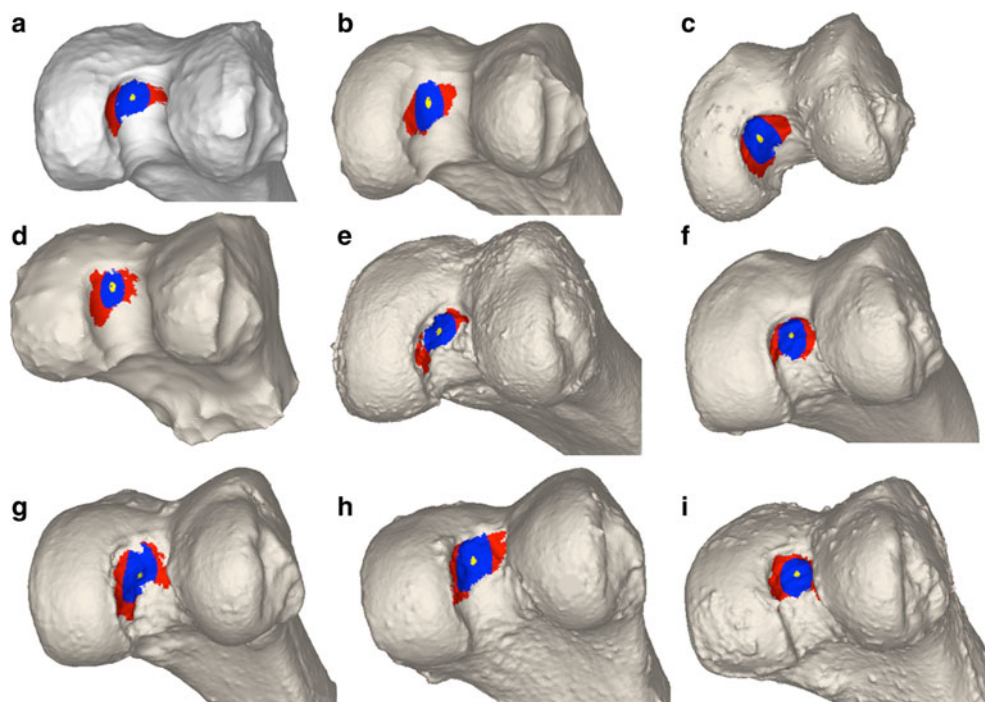


**Fig. 3** Three-dimensional representation of the femoral footprint of the native PCL (*red*) for the nine knees used (**a–i**). In *blue* colour, the intersection area of the best-fit PCL-cylinder superimposed on the femoral footprint (*red*), and in *yellow* colour, the osseous intersection of the central axis superimposed on preceding footprint and intersection area (*red* and *blue*)



#### Measurement of PCL footprint

Mean footprint surface area of the tibial and femoral footprint were  $189.1 \text{ mm}^2$  ( $\text{SD} \pm 63.0$ , range 68.6–263.4) and  $293.3 \text{ mm}^2$  ( $\text{SD} \pm 65.2$ , range 193.7–400.5), respectively. A high inter-patient variability was observed. No significant correlations were found between the femoral and the tibial footprint areas, the diameter of the native PCL in comparison with the femoral epicondylar width.

Spearman's rank correlation coefficient for the femoral footprint was 0.45 (n.s.); for the tibial footprint, 0.6 (n.s.); and for the native PCL diameter, 0.23 (n.s.).

#### Fitting of cylinders through the PCL

The mean diameter of the best-fit cylinder was  $10.5 \text{ mm} \pm 1.299$ . The mean coverage of the best-fit cylinder on the tibial and femoral footprint was  $76.5 \pm 11.7$

and  $46.5 \pm 6.3$  %, respectively. The best-fit cylinder central axis was located in the AL bundle footprint on the femur and more centrally in the PCL footprint on the tibia.

## Discussion

This study is the first to describe the detailed anatomy of the human PCL with respect to its course and footprints using a direct contrast-enhanced visualization methodology based on CT imaging in combination with a 3D approach. This unique approach offers valuable information on the bony insertion site but also offers new insights into optimal tunnel placement based on the new concept of best-fit tunnel and central axis. The latter technology is only possible through soft tissue visualization and allows maximum ligament soft tissue coverage in contrast to the mid-footprint anatomical approach which allows maximum bony footprint coverage. However, maximum footprint coverage does not necessarily encompass maximum soft tissue coverage. It is well known that the anterolateral bundle of the PCL is both functionally and anatomically more important [3]. A mid-footprint approach, however, will only incorporate equal parts of the AL and PM bundle and therefore underestimate the importance of the AL bundle [1–3, 5, 11, 13, 20]. In contrast, the best-fit cylinder approach would suggest a more balanced evaluation as it is not based on the mid-position of the footprints but rather on the bulk of the soft tissues of the PCL. Thus, since the bulk tissue of the AL bundle is larger than the PM bundle, the best-fit cylinder central axis will be closer to the AL bundle. This is confirmed by the observations made in this study. Nevertheless, while a mean best-fit cylinder of 10 mm diameter will cover almost 80 % of the tibial footprint, it will only cover 50 % of the femoral footprint. This observation suggests that single-bundle PCL reconstruction is never able to be considered anatomical on the femoral side [2, 8, 11, 12, 16, 18, 23, 24]. In addition, increasing the diameter of the PCL-cylinder in order to increase femoral footprint coverage would probably result in overstuffing the soft tissue compartment of the PCL and would result in impingement with the ACL.

This study also confirms the large difference between the tibial and the femoral footprint area with the former being significantly smaller. Nevertheless, the anatomy of the tibial footprint was characterized in all cases by 2 different planes. In contrast to a number of studies, we, however, were unable to discern the medial bifurcate ridge on the femur in between the AL and the PM bundle [7, 8]. In addition, a large inter-patient variability concerning footprint area is observed. Although most anatomical studies are limited by a low number of samples and thus low generalizability of these observations, such high

variability should be incorporated into the treatment algorithm of PCL reconstruction as it can influence the graft choice and graft diameter [1, 5, 9, 20].

## Conclusion

This study is the first to describe the detailed anatomy of the human PCL with respect to its course and footprints using a 3D approach. It confirms the large difference between the tibial and the femoral footprint area with the former being significantly smaller. In addition, a large inter-patient variability is observed. The best-fit cylinder and central axis concept offers additional insights to develop improved techniques for restoring the function of the native PCL.

## References

1. Amis AA, Gupte CM, Bull AM, Edwards A (2006) Anatomy of the posterior cruciate ligament and the menisofemoral ligaments. *Knee Surg Sports Traumatol Arthrosc* 14:257–263
2. Bergfeld JA, Graham SM, Parker RD, Valdevit ADC, Kambic HE (2005) A biomechanical comparison of posterior cruciate ligament reconstruction using single—and double-bundle tibial inlay technique. *Am J Sports Med* 33:976–981
3. Bowman KF Jr, Sekiya JK (2009) Anatomy and biomechanics of the posterior cruciate ligament and other ligaments of the knee. *Oper Tech Sports Med* 17:126–134
4. De Maeseneer M, Jager T, Vanderdood K, Van Roy P, Shahabpour M, Marcelis S (2003) Ultrasound during dissection of cadaveric specimens: a new method for obtaining ultrasound-anatomic correlations in musculoskeletal radiology. *Eur Radiol* 14:870–874
5. Edwards A, Bull AM, Amis AA (2007) The attachments of the fiber bundles of the posterior cruciate ligament: an anatomic study. *Arthroscopy* 23:284–290
6. Feigl G, Fuchs A, Gries M, Hogan QH, Weninger B, Rosmarin W (2006) A supraomohyoid plexus block designed to avoid complications. *Surg Radiol Anat* 28:403–408
7. Forsythe B, Harner C, Martins CA, Shen W, Lopes OV Jr, Fu FH (2009) Topography of the femoral attachment of the posterior cruciate ligament. Surgical technique. *J Bone Joint Surg Am* 91(1):89–100
8. Forsythe B, Kopf S, Wong AK, Martins CA, Anderst W, Tashman S, Fu FH (2010) The location of femoral and tibial tunnels in anatomic double-bundle anterior cruciate ligament reconstruction analyzed by three-dimensional computed tomography models. *J Bone Joint Surg Am* 92(6):1418–1426
9. Greiner P, Magnussen R, Lustig S, Demey G, Neyret P, Servien E (2011) Computed tomography evaluation of the femoral and tibial attachments of the posterior cruciate ligament in vitro. *Knee Surg Sports Traumatol Arthrosc* 19:1876–1883
10. Groscurth P, Egli P, Kapfhammer J, Rager G, Hornung JP, Fasel JDH (2001) Gross anatomy in the surgical curriculum in Switzerland: improved cadaver preservation, anatomical models, and course development. *Anat Rec (New Anat)* 265:254–256
11. Hatayama K, Higuchi H, Kimura M, Kobayashi Y, Asagumo H, Takagishi K (2006) A comparison of single—and double-bundle

- posterior cruciate ligament reconstruction: review of 20 cases. *Am J Orthop* 25:568–571
12. Kohen RB, Sekiya JK (2009) Single-bundle versus double-bundle posterior cruciate ligament reconstruction. *Arthroscopy* 25:1470–1477
  13. Lorenz S, Elser F, Brucker PU, Obst T, Imhoff AB (2009) Radiological evaluation of the anterolateral and posteromedial bundle insertion sites of the posterior cruciate ligament. *Knee Surg Sports Traumatol Arthrosc* 17:683–690
  14. Martelli S, Zaffagnini S, Bignozzi S, Lopomo NF, Lacono F, Marcacci M (2007) KIN-Nav navigation system for kinematic assessment in anterior cruciate ligament reconstruction: features, use, and perspectives. *Proc Inst Mech Eng H* 221(7):725–737
  15. Morgan CD, Kalman VR, Grawl DM (1997) The anatomic origin of the posterior cruciate ligament: where is it? reference landmarks for PCL reconstruction. *Arthroscopy* 13:325–331
  16. Petersen W, Lenschow S, Weimann A, Strobel MJ, Raschke MJ, Zantop T (2006) Importance of femoral tunnel placement in double-bundle posterior cruciate ligament reconstruction: biomechanical analysis using a robotic/universal force-moment sensor testing system. *Am J Sports Med* 34:456–463
  17. Pfirrmann CW, Oberholzer PA, Zanetti M, Boos N, Trudell DJ, Resnick D, Hodler J (2001) Selective nerve root blocks for the treatment of sciatica: evaluation of injection site and effectiveness. A study with patients and cadavers. *Radiology* 221:704–711
  18. Shearn JT, Grood ES, Noyes FR et al (2004) Two-bundle posterior cruciate ligament reconstruction: how bundle tension depends on femoral placement. *J Bone Joint Surg Am* 79:381–386
  19. Tajima G, Nozaki M, Iriuchishima T, Ingham SJ, Shen W, Smolinski P, Fu FH (2009) Morphology of the tibial insertion of the posterior cruciate ligament. *J Bone Joint Surg Am* 91(4): 859–866
  20. Takahashi M, Matsubara T, Doi M, Suzuki D, Nagano A (2006) Anatomical study of the femoral and tibial insertions of the anterolateral and posteromedial bundles of human posterior cruciate ligament. *Knee Surg Sports Traumatol Arthrosc* 14:1055–1059
  21. Van Dommelen BA, Fowler PJ (1989) Anatomy of the posterior cruciate ligament. A review. *Am J Sports Med* 17:24–29
  22. Van Hoof T, Gomes GT, Audenaert E, Verstraete K, Kerckaert I, D’Herde K (2008) 3D computerized model for measuring strain and displacement of the brachial plexus following placement of reverse shoulder prosthesis. *Anat Rec (Hoboken)* 291:1173–1185
  23. Wang CJ, Weng LH, Hsu CC, Chan YS (2004) Arthroscopic single- versus double-bundle posterior cruciate ligament reconstruction using hamstring autograft. *Injury* 35:1293–1299
  24. Yasuda K, van Eck CF, Hoshino Y, Fu FH, Tashman S (2011) Anatomic single- and double-bundle anterior cruciate ligament reconstruction, part 1: basic science. *Am J Sports Med* 39(8): 1789–1799